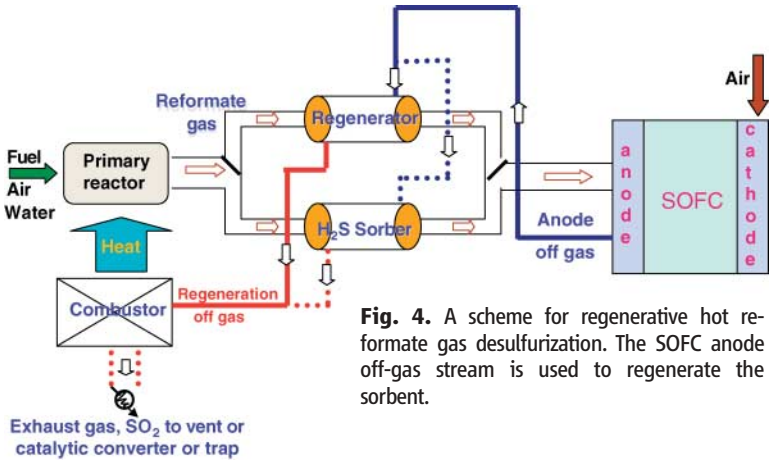

Fig. 4. A scheme for regenerative hot reformate gas desulfurization. The SOFC anode off-gas stream is used to regenerate the sorbent.

otherwise would be trapped or converted as appropriate.

Figure 4 shows a conceptual flowchart of fuel reforming for SOFC use, including regenerative desulfurization over a lanthanide oxide sorbent in the temperature range of 650° to 800°C. This shows that all of the SOFC anode off-gas stream can be used to regenerate the sorbent surface. That is, no split streams are required, because regeneration can take place at high space velocity that corresponds to using the whole anode off-gas stream over the saturated sorbent. This design also avoids the use of a new gas stream, such as air and its attending compressor equipment, for the regeneration step. The dual sorber and regenerator units can be made as small as desired for different applications. In certain designs, some of the anode off-gas may be directed straight to the reformer to add steam to the fuel-reforming process. In such cases, a split stream of the anode off-gas would be used to regenerate the sorbent units.

Various configurations of reactors can be envisioned for the desulfurization system. Because of its low pressure drop, a ceramic honeycomb monolith with the sorbent coated as a thin layer on the channel walls is considered a suitable choice. Sizing the reactor volume for a 5–kilowatt electric (kWe)–rated SOFC, at a 400,000 $hour^{-1}$ space velocity, a 0.2-liter monolith (0.02-liter sorbent) can be used in each of the two (sorber and regenerator) units (*16*). The corresponding switch time for a gas containing 500 to 50 ppm H_2S would be 0.5 to 5 min, respectively (*16*). For a first-order process, the lower the content of H_2S in the fuel gas, the lower the sulfur capacity will be. This was not considered in the above estimate because a compensating effect can come from the use of sorbents with much higher surface area than the one used here. The flexibility that this design entails should be of interest to any scale of power generation, but more importantly to limited-footprint applications, such as auxiliary power units, portable fuel cells, and confined-space installations.

References and Notes

1. Z. Wang, M. Flytzani-Stephanopoulos, *Energy Fuels* **19**, 2089 (2005).
2. I. Barin, F. Sauert, E. Schultze-Rhonhof, S. S. Wang, *Thermochemical Data of Pure Substances Part I/Part II* (Verlag Chemie, Weinheim, Germany, 1993).
3. I. Barin, O. Knacke, *Thermochemical Properties of Inorganic Substances* (Springer-Verlag, New York, 1973).
4. I. Barin, O. Knacke, O. Kubaschewski, *Thermochemical Properties of Inorganic Substances: Supplement* (Springer-Verlag, New York, 1977).
5. S. Lew, A. F. Sarofim, M. Flytzani-Stephanopoulos, *Ind. Eng. Chem. Res.* **31**, 1890 (1992).
6. Z. Li, M. Flytzani-Stephanopoulos, *Ind. Eng. Chem. Res.* **36**, 187 (1997).
7. M. Kobayashi, M. Flytzani-Stephanopoulos, *Ind. Eng. Chem. Res.* **41**, 3115 (2002).
8. J. H. Swisher, J. Yang, R. P. Gupta, *Ind. Eng. Chem. Res.* **34**, 4463 (1995).
9. R. V. Siriwardane, J. A. Poston, G. Evans, *Ind. Eng. Chem. Res.* **33**, 2810 (1994).
10. M. Kobayashi, H. Shirai, M. Nunokawa, *Ind. Eng. Chem. Res.* **41**, 2903 (2002).
11. E. Garcia, J. M. Palacios, L. Alonso, R. Moliner, *Energy Fuels* **14**, 1296 (2000).
12. K. W. Yi, E. Podlaha, D. P. Harrison, *Ind. Eng. Chem. Res.* **44**, 7086 (2005).
13. W. J. W. Bakker, F. Kapteijn, J. A. Moulijn, *Chem. Eng. J.* **96**, 223 (2003).
14. M. Flytzani-Stephanopoulos, Z. Wang, M. Sakbodin, PCT Patent Application No. PCT/US05/40488; filed 8 November 2005.
15. Materials and methods are available as supporting material on *Science* Online.
16. Approximately 50 liters/min H_2 (STP) per 5 kWe is required for a Polymer Electrolyte Membrane (PEM) fuel cell (*17*). Taking this as the basis for an SOFC, a flow rate of 125 liters/min reformate gas with 40% H_2 will be required to power a 5-kWe SOFC. At space velocity = 400,000 $hour^{-1}$, about 20 cm^3 of sorbent or 200 cm^3 monolith volume (larger by a factor of 10) will be required. For two units, 400 cm^3 would be required. The switching time, t, is estimated for a sorbent density of 2 g/cm^3 and for a surface sulfur capacity of 1 mg $S/g_{sorbent}$. Based on the mass balance, the following equation can be established: $(500 \text{ or } 50 \times 10^{-6}) \times 125$ liters/min $\times\ t = [1 \text{ mg S/g}_{sorbent} (2 \text{ g/cm}^3 \times 20 \text{ cm}^3)]/32{,}000$ mg/mol $\times$ 22.4 liters/mol. Thus, $t = 0.5$ min for 500 ppm H_2S or 5 min for 50 ppm H_2S-laden fuel gas.
17. F. Barbir, *PEM Fuel Cells Theory and Practice* (Elsevier Academic Press, Burlington, MA, 2005).

18. This work was supported by the Army Research Laboratory, Power and Energy Collaborative Technology Alliances (CTA) program.

Supporting Online Material

www.sciencemag.org/cgi/content/full/312/5779/1508/DC1
Materials and Methods
Figs. S1 to S6
Table S1
References

1 February 2006; accepted 13 April 2006
10.1126/science.1125684

Near-Synchronous Interhemispheric Termination of the Last Glacial Maximum in Mid-Latitudes

Joerg M. Schaefer,[1]* George H. Denton,[2] David J. A. Barrell,[3] Susan Ivy-Ochs,[4,5] Peter W. Kubik,[6] Bjorn G. Andersen,[7] Fred M. Phillips,[8] Thomas V. Lowell,[9] Christian Schlüchter[10]

Isotopic records from polar ice cores imply globally asynchronous warming at the end of the last glaciation. However, ^{10}Be exposure dates show that large-scale retreat of mid-latitude Last Glacial Maximum glaciers commenced at about the same time in both hemispheres. The timing of retreat is consistent with the onset of temperature and atmospheric CO_2 increases in Antarctic ice cores. We suggest that a global trend of rising summer temperatures at the end of the Last Glacial Maximum was obscured in North Atlantic regions by hypercold winters associated with unusually extensive winter sea ice.

Terminations of asymmetric 100,000-year glacial cycles represent one of the most fundamental climate signals of late Quaternary time (*1*). Isotopic compositions in Antarctic ice cores and in benthic foraminifera from marine sediment cores show well-defined changes beginning between about 19×10^3 to 17×10^3 years ago (ka) (*2*), interpreted to represent the onset of the termination of the Last Glacial Maximum (LGM) (*3*–*7*). In contrast, Greenland ice cores register continued stadial cold conditions between 17 ka and 14.7 ka (*8*, *9*). At the same time, North Atlantic sediments reveal a major pulse of iceberg discharge (*10*) accompanied by a near-shutdown of the meridional overturning circu-

lation (MOC) (*11*). We used ^{10}Be chronologies of mid-latitude moraines to investigate this puzzle of asynchrony between Antarctic and Greenland climate signals early in the last termination. We focused on mid-latitude mountain valley glaciers and outlet glaciers of localized ice caps, rather than continental glaciers (e.g., the Cordilleran and Laurentide ice sheets). Moraines formed by glacier advance and retreat, reflecting variations in temperature and precipitation, sensitively record climate change [e.g., (*12*, *13*)]. Mid-latitude glacial deposits afford an opportunity to constrain interhemispheric comparisons of climate change. The LGM is represented in formerly glaciated regions by a prominent set of morphologically distinct moraines (Fig. 1 and figs. S1 and S2). Within the last decade, surface exposure dating (SED), by measurement of in situ–produced cosmogenic nuclides in boulders on moraine surfaces, has afforded new capabilities for quantifying glacial histories (*14*).

We present a compilation of new and published ^{10}Be data from deposits formed at the start of the termination of the LGM, focusing on a comparison of the inner LGM moraines in southern and northern mid-latitudes. Buildup of ^{10}Be in surface boulders is assumed to have commenced as soon as glaciers retreated from these inner moraines. In each region, we infer that such recession marks the onset of the last termination. The key questions we investigate are as follows: (i) When did the LGM termination begin in the mid-latitudes of both hemispheres? (ii) How does the timing of this termination compare to events recorded in polar ice cores? (iii) Do the mid-latitudes yield evidence that may help to solve the puzzle of interpolar asynchrony during the early part of the last termination?

From southern mid-latitudes, we present a glacial geomorphology map (Fig. 1) and ^{10}Be chronology (table S1) from Lake Pukaki, Southern Alps, New Zealand. We then compare the ^{10}Be results with previously published moraine chronologies from southeastern Australia (*15*, *16*) and Lago Buenos Aires in northern Patagonia (*17*). The moraine chronologies from northern mid-latitudes include new ^{10}Be data from Bloody Canyon on the eastern flank of the Sierra Nevada (fig. S2 and table S2), together with published chronologies from the Fremont Lake basin in the Wind River Range of Wyoming (*18*), the Wallowa Mountains in Oregon (*19*), and the northern Yellowstone ice cap in Montana (*20*), all in the United States of America. We also discuss published ^{10}Be dates from moraines in northern Switzerland (*21*). For details of all field sites, see Supporting Online Material (SOM) Text.

Characteristically, mid-latitude LGM glacial sequences were deposited by large, low-gradient valley glacier systems that formed well-preserved moraine belt(s) that are several kilometers wide. Substantial lakes commonly lie inboard of the inner LGM moraine(s), attesting to notable glacier retreat at the LGM termination. In these settings, the most precise moraine chronology records are from New Zealand (Fig. 1 and fig. S1), southeastern Australia (*15*, *16*), Wind River Range (*18*), and Wallowa Mountains (*19*). Other

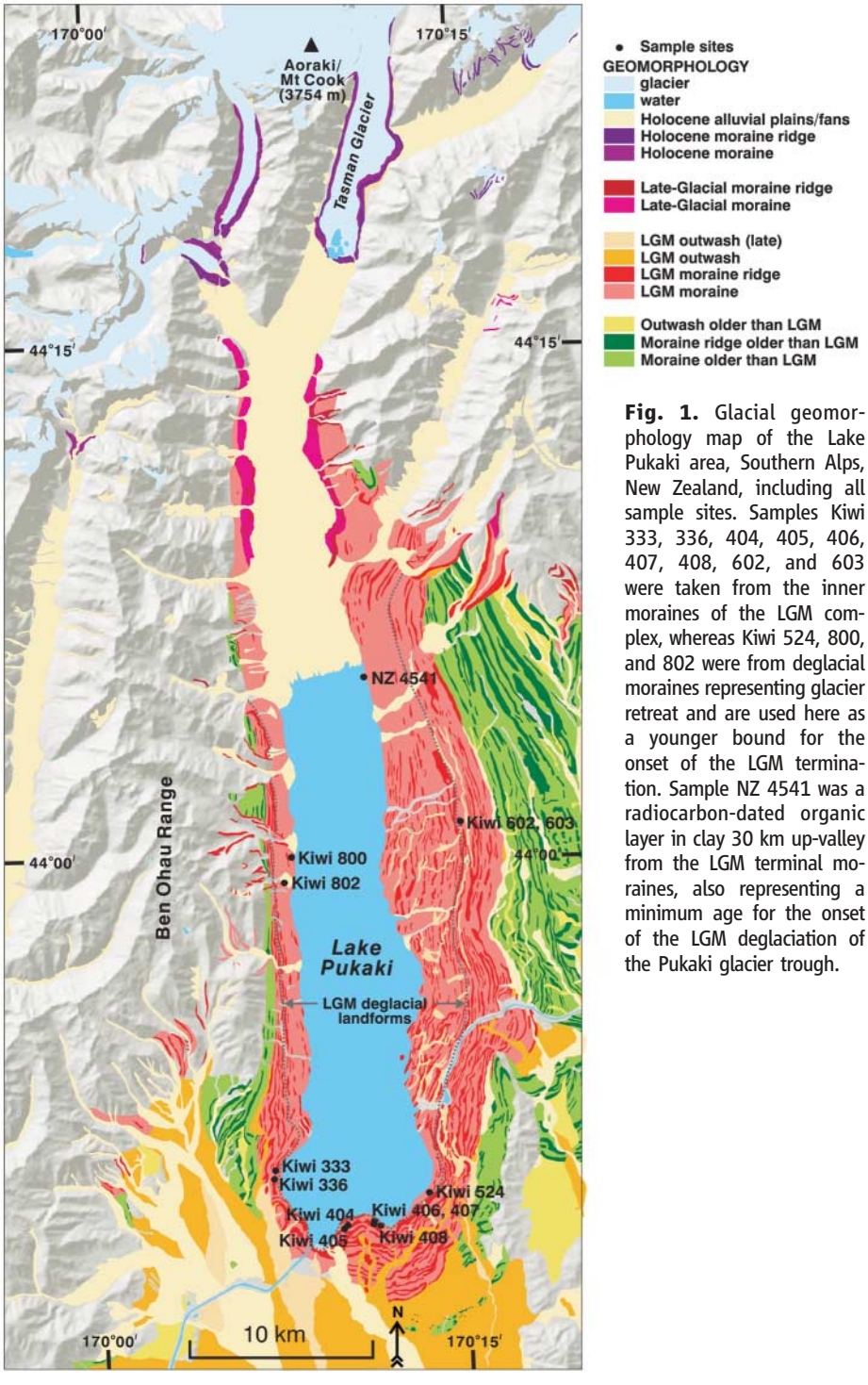

Fig. 1. Glacial geomorphology map of the Lake Pukaki area, Southern Alps, New Zealand, including all sample sites. Samples Kiwi 333, 336, 404, 405, 406, 407, 408, 602, and 603 were taken from the inner moraines of the LGM complex, whereas Kiwi 524, 800, and 802 were from deglacial moraines representing glacier retreat and are used here as a younger bound for the onset of the LGM termination. Sample NZ 4541 was a radiocarbon-dated organic layer in clay 30 km up-valley from the LGM terminal moraines, also representing a minimum age for the onset of the LGM deglaciation of the Pukaki glacier trough.

[1]Lamont-Doherty Earth Observatory (L-DEO), Palisades, NY 10964, USA. [2]Department of Earth Sciences and Climate Change Institute, University of Maine, Orono, ME 04469, USA. [3]GNS Science, Dunedin, New Zealand. [4]Institute of Particle Physics, Eidgenössiche Technische Hochschule (ETH) Hoenggerberg, 8093 Zürich, Switzerland. [5]Geographisches Institut, Universität Zürich-Irchel, CH-8057 Zürich, Switzerland. [6]Paul Scherrer Institute, c/o Institute of Particle Physics, ETH-Hoenggerberg, 8093 Zürich, Switzerland. [7]University of Oslo, 0316 Oslo, Norway. [8]New Mexico Tech, Soccorro, NM 87801, USA. [9]University of Cincinnati, Cincinnati, OH 45221, USA. [10]Universität Bern, Geologisches Institut, CH-3012 Bern, Switzerland.

*To whom correspondence should be addressed. E-mail: schaefer@ldeo.columbia.edu

locations discussed here display either closely clustered moraines [e.g., Yellowstone Ice Cap (*20*)] or a single prominent moraine representing the late LGM [e.g., Bloody Canyon (fig. S2)]. In the latter case, LGM moraine formation was predominantly by vertical accretion, with the earlier LGM tills lying buried in the moraine core and the youngest LGM tills forming the ground surface. For all sites except northern Switzerland, the sampled boulders lie on the inner moraines adjacent to an LGM glacier trough that was evacuated by ice at the beginning of the termination. The Swiss study (*21*) provided a chronology for an outermost LGM moraine, thus yielding a maximum age constraint on the last termination.

The 64 ^{10}Be dates used for this mid-latitude review are summarized in Table 1 and Fig. 2 (the dates are listed individually in tables S1 to S3, the latter including an additional 41 ^{10}Be dates from tropical regions). The internal consistency between the ^{10}Be chronologies from the various mid-latitude inner LGM moraines is striking on the basis of both mean values and oldest values of the respective age populations (*14*). The Southern Hemisphere mean SED ages for the onset of the LGM termination are 16.8 × 10^3 years (ky) [southeastern Australia (*15*, *16*)], 17.4 ky [Lago Buenos Aires, Patagonia (*17*)], and 17.4 ky (Lake Pukaki, New Zealand). The Patagonian study is based on only two samples and thus is complemented by the LGM chronology from the nearby Chilean Lake District (42°S, 73°W) (*13*). On the basis of geomorphic mapping and a detailed radiocarbon chronology of glacial deposits, we dated the beginning of the last termination in the Chilean Lake District at 14,700 carbon-14 years before the present (^{14}C yr B.P.) (*22*), corresponding to about 17,900 calendar years (IntCal04). The overall mean of these ages is 17.3 ky.

The ^{10}Be exposure ages of inner LGM moraines in the Northern Hemisphere range from 16.3 ky [northern Yellowstone Ice Cap (*20*)] to 17.8 ky (Bloody Canyon, Sierra Nevada). The ^{10}Be ages from the terminal LGM moraine at Bloody Canyon, the Tioga 3 moraine, agree with earlier ^{36}Cl chronologies given in (*23*) (table S4). The northern Yellowstone data afford the youngest ages in this survey. However, recently published ^{10}Be dates from eastern Yellowstone Ice Cap moraines yield ages that are 5 to 10% older (*24*). For the conclusions drawn below it is not critical whether the northern Yellowstone data are included, but we consider it appropriate for consistency to retain them in the evaluation. Compatible with the geomorphic position of the sampled boulders, the ^{10}Be dates from the outer LGM moraines of the Rhone Glacier system at Wangen an der Aare, northern Switzerland (*21*), yield the oldest mean age of 19.3 ± 1.8 ky, representing an older bound for the termination. A close minimum age for the last termination of 14,600 ^{14}C yr B.P., corresponding to 17,700 calendar years, was reported by Lister *et al.* (*25*) from a sediment core in nearby Lake Zurich on the basis of a twig recovered just above an ice-rafted sediment layer deposited when the ice evacuated the basin. The Northern Hemisphere mean of SED ages for the onset of the termination, including the northern Yellowstone data, is 17.1 ky. Excluding the northern Yellowstone data, the mean is 17.4 ky: Both are indistinguishable from the Southern Hemisphere mean of 17.3 ky.

Table 1. Comparison of ^{10}Be data for the inner LGM moraines in southern and northern mid-latitudes. Means are nonweighted; uncertainties are 1σ standard deviation. The SH mean and the NH mean represent the mean and the 1σ standard deviation of the mean ages of each individual study in the respective hemisphere. We include the oldest age of the age populations from each locality as a conservative maximum for the formation age of the respective moraine (*14*).

Site	Position	Mean age (ky)	"Oldest" age (ky)	Comment	Reference
		Southern Hemisphere			
Lake Pukaki, New Zealand	44°S/170°E 550–770 m	17.4 ± 1.0	19.3 ± 1.0	Seven samples (table S1)	This study
Southeastern Australia	36°–43°S/145°–148°E 600–2000 m	16.8 ± 1.3	19.1 ± 1.8	19 samples	(*15*, *16*)
Lago Buenos Aires, Patagonia	46.5°S/71°W 430–455 m	17.4 ± 1.9	18.8 ± 1.5	Two samples	(*17*)
Chilean Lake District	41°S/73°W	17.9 ± 0.4		72 ^{14}C calibrated ^{14}C age	(*22*)
SH mean		17.3 ± 0.5	19.1 ± 0.3		
		Northern Hemisphere			
Bloody Canyon, Sierra Nevada	38°N/119°W 2350–2450 m	17.8 ± 1.5	19.7 ± 1.2	Four samples (table S2)	This study
Fremont Lake Basin, Wind River Range, Wyoming	43°N/109°W 2250–2400 m	17.6 ± 0.8	18.7 ± 0.6	10 samples	(*18*)
Wallowa Mountains, Oregon	45°N/117°W 1400–1560 m	16.8 ± 0.8	18.0 ± 0.8	9 samples out of 15	(*19*)
Northern Yellowstone Ice Cap, Montana	45°N/111°W 1530–1560 m	16.3 ± 1.2	18.8 ± 1.6	Nine samples	(*20*)
Northern Switzerland	47°N/8°E 580–610 m	19.3 ± 1.8	20.9 ± 0.9	Four samples	(*21*)
NH mean		17.1 ± 0.7	18.8 ± 0.7	Including Yellowstone	
		(17.4 ± 0.5)	(18.8 ± 0.9)	(Excluding Yellowstone)	

The timing of the beginning of the LGM termination of mid-latitude glaciers shows remarkable regional, hemispheric, and interhemispheric consistency despite the varied geographic, geological, glaciological, and microclimatic settings. Therefore, we conclude that the climate change driving the termination was of interhemispheric character. A recent study from the tropics further strengthens this conclusion. Smith *et al.* (*26*) reported ^{10}Be dates of moraines in Peru (5°S) and Bolivia (15°S). They showed an early LGM maximum extent before marine isotope stage 2, but the innermost LGM termination moraines yielded a nonweighted mean of 17.3 ± 1.9 ky (41 of 50 samples from six moraines, i.e., nine outliers excluded; table S3), indistinguishable from the mid-latitude data (Table 1).

Although reduced annual precipitation could have triggered LGM glacier retreat, large spatial and temporal variabilities in precipitation patterns imply that very complex changes in atmospheric circulation are needed to account for a uniform interhemispheric change in precipitation. However, glacier mass balance is highly sensitive to temperature during the summer ablation season and much less responsive to winter temperatures [e.g., (*27*)]. A striking consistency between temperature rise since the middle of the 19th century and retreat of 169 different glacier systems from Little Ice Age moraines (*28*) highlights glacier sensitivity to temperature changes. The retreat of LGM ice and abandonment of LGM moraines had many morphological similarities, albeit on a much larger scale, to the present-day glacier recession from Little Ice Age moraines. We conclude that global rise in summer temperatures provides a straightforward explanation for the observed synchronous interhemispheric, mid-latitude glacier retreat at the end of the LGM.

The onset of the LGM termination in mid-latitude moraines and in polar ice core records is compared in Fig. 2. A warming trend began in Antarctica sometime between 19 ky and 17 ky ago (*2*, *5*). The start of mid-latitude LGM glacier termination in both hemispheres is

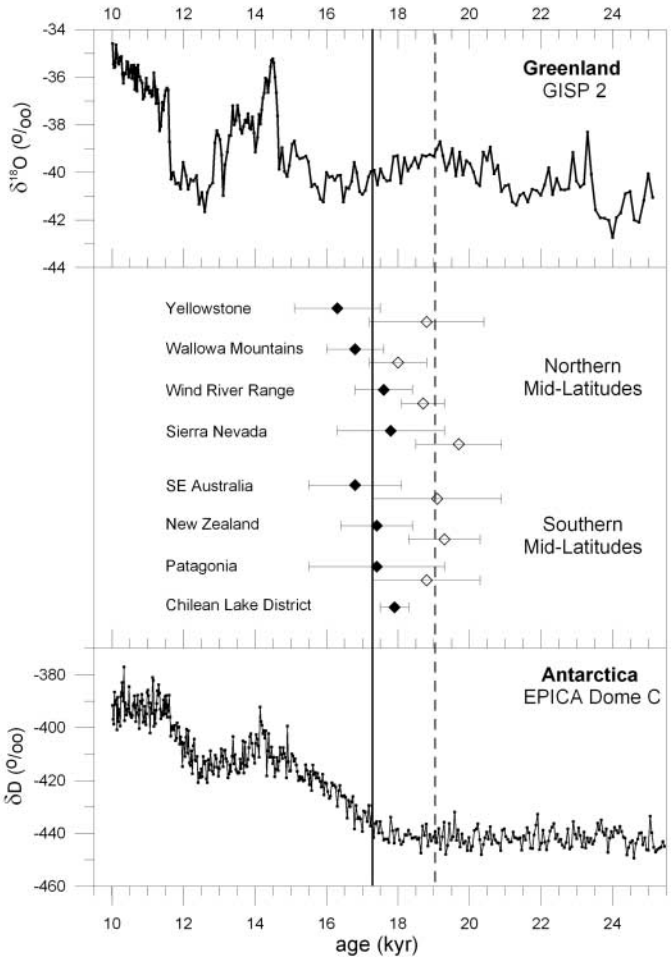

Fig. 2. Comparison of the onset of the mid-latitude glacier LGM termination with polar ice core records. Plotted for each moraine record are (i) the mean age (solid diamonds) and (ii) the oldest ^{10}Be boulder age of each moraine set (open diamonds). Error bars indicate 1σ standard deviation and 1σ analytical uncertainty, respectively. The solid vertical line is the mean of all individual mean ages (17.2 ky); the dotted vertical line is the mean age of all the oldest ^{10}Be ages [19 ky, see text and (*14*)]. No substantial warming was indicated in the isotopic record from Greenland at that time (*8*), whereas isotopes implied that temperatures started to rise in Antarctica (*5*) in near-synchrony with the onset of mid-latitude glacier LGM termination.

concordant with steadily rising temperatures recorded in Antarctica and also correlates well with the onset of the glacial-interglacial transition defined by benthic foraminifera records [e.g., (*7*)]. In near-synchrony with temperature increase, Antarctic ice core greenhouse gas concentrations also started to rise [e.g., (*29*)], implying that CO_2 could have been the globalizer of the LGM termination.

The paleoclimate records in the North Atlantic region tell a very different story during the glacial-interglacial transition (Fig. 2). Slight temperature rise may have begun in Greenland as early as 24 ka (*30*), but the dramatic warming event at the onset of the Bölling occurred at 14.7 ka (*31*), unambiguously later than the mid-latitude glacier termination of the LGM. Similarly, marine sediment records show that the MOC in the North Atlantic almost shut down between 17.5 ka and 14.7 ka (*11*), which is consistent with sea surface cooling [e.g., (*32*)] and a continuation of cold stadial conditions in Greenland (*9*) during this interval. Thus, the Greenland ice cores do not express the interhemispheric summer temperature rise at the beginning of the last termination, evident in mid-latitude moraine records.

On the basis of our data, we extend the reasoning given in (*33*) and suggest the following hypothesis to explain this anomaly. During the LGM, large volumes of ice were stored in Northern Hemisphere ice sheets. A global summer temperature warming initiated mid-latitude glacier retreat and also destabilized the Northern Hemisphere ice sheets, particularly the seaward-draining ice streams, triggering large-scale iceberg discharge into the North Atlantic commencing at about 17.5 ka (*10*). The resulting freshwater input to the North Atlantic zone of deep-water formation slowed and almost stopped MOC (*11*), resulting in a substantial spread of North Atlantic sea winter ice. As a consequence of an extensive sea-ice cover, the North Atlantic climate between about 17.5 and 14.7 ka (i.e., early in the LGM termination) was characterized by hypercold winters (*33*), which markedly reduced mean-annual temperatures and obscured the global summer temperature increase registered by mid-latitude glacier recession. By this scenario, the Greenland isotopic records attest to regional North Atlantic conditions during a termination that was nearly global in character.

References and Notes

1. W. S. Broecker, J. van Donk, *Rev. Geophys. Space Phys.* **8**, 169 (1970).
2. Because of the use of different age models, the onset of the last termination in Antarctic ice cores has been assigned ages of about 19 ky for Byrd [Greenland Ice Sheet Project (GISP) 2 chronology] (*3*), 18 ky for the Byrd core [Greenland Ice Core Project (GRIP) chronology] (*4*), 17.5 ky for European Project for Ice Coring in Antarctica (EPICA) Dome C (EDC1 time scale) (*5*), and 17 ky for Vostok (GT4 time scale) (*6*).
3. T. Blunier, E. J. Brook, *Science* **291**, 109 (2001).
4. T. Blunier *et al.*, *Nature* **394**, 739 (1998).
5. J. Jouzel *et al.*, *Geophys. Res. Lett.* **28**, 3199 (2001).
6. J. R. Petit *et al.*, *Nature* **399**, 429 (1999).
7. N. J. Shackleton *et al.*, *Nature* **335**, 708 (1988).
8. M. Stuiver, P. M. Grootes, *Quat. Res.* **53**, 277 (2000).
9. This period is called Greenland Stadial 2a by (*34*) and corresponds to the European Oldest Dryas interval.
10. G. C. Bond, R. Lotti, *Science* **267**, 1005 (1995).
11. J. F. McManus, R. Francois, J.-M. Gherardi, L. D. Keigwin, S. Brown-Leger, *Nature* **428**, 834 (2004).
12. C. M. Clapperton, *Quat. Sci. Rev.* **9**, 299 (1990).
13. G. H. Denton, Ed., *Geogr. Annal.* **81A**, 105 (1999).
14. Materials and methods are available as supporting material on *Science* Online.
15. T. T. Barrows, J. O. Stone, L. K. Fifield, R. G. Cresswell, *Quat. Sci. Rev.* **21**, 159 (2002).
16. T. T. Barrows, J. O. Stone, L. K. Fifield, R. G. Cresswell, *Quat. Res.* **55**, 179 (2001).
17. M. R. Kaplan, R. P. Ackert, B. S. Singer, D. C. Douglass, M. D. Kurz, *Geol. Soc. Am. Bull.* **116**, 308 (2004).
18. J. C. Gosse, J. Klein, E. B. Evenson, B. Lawn, R. Middleton, *Science* **268**, 1329 (1995).
19. J. M. Licciardi, P. U. Clark, E. J. Brook, D. Elmore, P. Sharma, *Geology* **32**, 81 (2004).
20. J. M. Licciardi *et al.*, *Geology* **29**, 1095 (2001).
21. S. Ivy-Ochs, J. M. Schaefer, P. W. Kubik, H.-A. Synal, C. Schlüchter, *Eclogae Geol. Helv.* **97**, 47 (2004).
22. G. H. Denton *et al.*, in (*13*), p. 107.
23. F. M. Phillips *et al.*, *Science* **274**, 749 (1996).
24. J. M. Licciardi, K. L. Pierce, M. D. Kurz, R. C. Finkel, *Geol. Soc. Am. Abstr. Prog.* **37**, 41 (2005).
25. G. Lister, *J. Quat. Sci.* **7**, 187 (1988).
26. J. A. Smith, G. O. Seltzer, D. L. Farber, D. T. Rodbell, R. C. Finkel, *Science* **308**, 678 (2005).
27. J. Oerlemans, *Glaciers and Climate Change*, A. A. Balkema Publishers, Ed. (Lisse, Netherlands, 2001), pp. 148.
28. J. Oerlemans, *Science* **308**, 675 (2005); published online 3 March 2005 (10.1126/science.1107046).
29. E. Monnin *et al.*, *Science* **291**, 112 (2001).
30. R. B. Alley, E. J. Brook, S. Anandakrishnan, *Quat. Sci. Rev.* **21**, 431 (2002).
31. J. P. Severinghaus, E. J. Brook, *Science* **286**, 930 (1999).
32. E. Bard, F. Rostek, J.-L. Turon, S. Gendreau, *Science* **289**, 1321 (2000).
33. G. H. Denton, R. B. Alley, G. C. Comer, W. S. Broecker, *Quat. Sci. Rev.* **24**, 1159 (2005).
34. M. J. C. Walker *et al.*, *Quat. Sci. Rev.* **18**, 1143 (1999).

35. J.M.S. thanks the Comer Science and Educational Foundation and the Lamont Climate Center for support of this study. GNS Science contributed to the glacial geomorphic mapping in New Zealand and the participation of Barrell. NOAA supported the participation of G.H.D., B.G.A., and T.V.L. C.S. thanks the Schweizer Nationalfonds. We are grateful to V. Rinterknecht and R. Schwartz for help with the ^{10}Be samples from New Zealand and California and thank J. Licciardi, G. Winckler, B. Newton, and two anonymous reviewers for constructive comments. This is L-DEO contribution number 6898.

Supporting Online Material

www.sciencemag.org/cgi/content/full/312/5779/1510/DC1
Materials and Methods
SOM Text
Figs. S1 to S3
Tables S1 to S4
References

21 November 2005; accepted 25 April 2006
10.1126/science.1122872

Supporting Online Material for

Near-Synchronous Mid-Latitude Interhemispheric Termination of the Last Glacial Maximum

Joerg M. Schaefer,* George H. Denton, David J. A. Barrell, Susan Ivy-Ochs, Peter W. Kubik, Bjorn G. Andersen, Fred M. Phillips, Thomas V. Lowell, Christian Schlüchter

*To whom correspondence should be addressed. E-mail: schaefer@ldeo.columbia.edu

Published 9 June 2006, *Science* **312**, 1510 (2006)
DOI: 10.1126/science.1122872

This PDF file includes:

Supporting Online Material

Materials and Methods

^{10}Be-dating of moraine records

Reviews of the method of surface exposure dating (SED) using cosmogenic nuclides are given in (S*1*-*S4*). In this manuscript, we focus on in-situ ^{10}Be data, because ^{10}Be is generally considered the most reliable cosmogenic nuclide for SED on timescales discussed here, primarily due to well-calibrated production rates and high analytical precision. All ^{10}Be ages given here are normalized to the following set of parameters (Tables S1, S2, and S3): (i) sea-level/high-latitude production rate of 5.1 at g^{-1} yr^{-1} (S*5*); (ii) scaling for altitude and latitude is based on the standard atmosphere altitude-air pressure relation and follows the protocol given in (S*5*), which is essentially the scaling given in (S*4*) but includes updated scaling factors for production by muons; (iii) production rate corrections for sample thickness assuming exponential decrease of the production rate with depth (attenuation length Λ=150g cm^{-2}, rock density ρ=2.7 g cm^{-3}, unless otherwise stated in the original publication); (iv) production rate corrections for landscape shielding and/or dip of the sampled surface were applied where applicable as cited in the original references and for the new ^{10}Be data following (S*6*); (v) erosion is assumed to be negligible (a typical erosion rate cited is 1 mm/kyr, which would not affect the exposure ages significantly (<5%)); (vi) no corrections for paleomagnetic intensity variations have were applied, because the earth's magnetic field earlier in the Holocene was significantly stronger than today and was weaker than today during late glacial/LGM time; the integrated effect of these changes is nearly zero for samples within the age ranges considered here (~15-20 kyr); (vii) no corrections for boulder symmetries as proposed in (S*7*) were applied, because the suggested correction factors remain controversial and because large cubic boulders were sampled in the middle of the flat top surface (e.g. New Zealand) or boulder geometries are not documented.

Various geomorphologic processes can produce exposure ages that are too young (erosion, snow-cover, and post-depositional exhumation of boulders), whereas only exposure of the sample prior to deposition yields an older-than-deposition age. The latter case can be discounted if there is a cluster of boulder ages from one moraine, because pre-exposure typically affects individual rocks very differently, producing distinct outliers. Although we consider it unlikely that the processes of erosion, snow-cover or post-depositional exhumation were significant for the samples included in this review, we include the oldest age of each age population as a conservative older limit for the formation age of the respective moraine. Note that the agreement between the different ^{10}Be chronologies is striking for the oldest values and the mean values. This suggests that the variability within these data sets may be dominated by analytical errors rather than by geomorphological processes.

Accuracy of the surface exposure dating method

It remains controversial whether the SED method is accurate enough to resolve events on the sub-millennial time-scale. However, the overall precision of the internally consistent ^{10}Be data sets summarized in this study is commensurate with the precision required for the conclusions drawn in this study (Table 1, Fig. 2). Further, several of the SED data sets discussed show consistency with independent radiocarbon chronologies of organic deposits (New Zealand, Patagonia, Switzerland; see text).

Supporting Text

Short description of the geological setting of the moraine sets included in this study

The end of the LGM climate phase in the mid-latitude moraine record

We describe the geomorphologic setting for the new data sets from Lake Pukaki in New Zealand and Bloody Canyon in the eastern Sierra Nevada, US. For the published data sets discussed, we give the respective references below.

1. Southern mid-latitude glaciers

Lake Pukaki, Southern Alps, New Zealand

Lake Pukaki lies on the eastern side of the Southern Alps. Outside the margins of the lake, LGM moraines form a 1-to-5km-wide belt of lateral and terminal glaciogenic landforms, comprising a complex array of discontinuous moraine ridges, meltwater channels and outwash plains (see Fig. 1, Fig. S1) and (S*8*)). Up to at least 30 successive separate moraine ridges are preserved in the LGM landform complex, indicating many episodes of ice-front advance, stability and retreat. On the inboard side of the LGM moraine complex, a suite of deglacial moraines and multiple levels of kame terraces drape the margins of the evacuated LGM glacier trough that is occupied by Lake Pukaki. These deglacial features formed during the last major ice retreat from the LGM moraine complex.

An organic layer in clay, ponded behind a deglacial meltwater channel, lies 30 km up-valley from the LGM end moraines and 400 m below the highest adjacent deglacial moraines. The sample site now lies below the artificially raised level of Lake Pukaki (NZ 4541, Fig. 1). It has a ^{14}C age of 13,500 ± 250 years BP (S*9*), corresponding to an IntCal04 calibrated age of 16,033 ± 735 years BP and gives a minimum age for extensive downwasting and associated recession during LGM deglaciation of the Pukaki glacier trough.

Large boulders are common on the LGM moraines, and are predominantly hard, quartzo-feldspathic, fine-grained greywacke sandstone (Fig. S3). This lithology can be assumed to be very

resistant to erosion but it is difficult to process for cosmogenic ^{10}Be, primarily because it is not possible to clean the quartz to levels required by standard processing protocols without digesting most of the quartz. Accordingly, we had to process relatively large quartz samples. The processing protocol had to be adjusted to each sample during both the sequential leaching and decontamination of quartz from the rock matrix and the subsequent extraction of beryllium from the quartz separate.

We give dates for the inner moraine ridges of the LGM complex, outboard of the deglacial landform complex, as well as for moraines within the deglacial landforms (Fig. 1). ^{10}Be ages for these samples are shown in Table S1. Samples Kiwi 800 and 802 lie 100 to 200 m below the crest of the deglacial landform complex, thus were deposited after there had been considerable downwasting of the LGM glacier. Together with sample Kiwi 524, near the outer margin of the deglacial landform complex, these three dates yield a minimum age for the onset of deglaciation. Accordant to their stratigraphic position, their mean ^{10}Be-age of 15.4 ± 1.2 kyr is younger than those from boulders on the moraine ridges immediately outboard of the deglacial landforms and is compatible with the ^{14}C age given above. The ages for these boulders range from 15.0 kyr (Kiwi 405) to 19.1 kyr (Kiwi 406). Given the smaller size and thus lower quality of sample Kiwi 405 compared to its near neighbors Kiwi 404, 406 and 408, we consider the lower age of 405 to be an effect of a post-depositional process such as boulder-exhumation, erosion, or spalling. We therefore base our mean value on samples Kiwi 333, 336, 404, 406, 407, 408, 602, and 603, yielding a mean deposition age of 17.4 ± 1.0 kyr. As these samples come from just outside the LGM deglacial moraine complex, they provide a closely limiting maximum age for the LGM termination at this location. Note that including Kiwi 405 would alter the mean value to 17.1 ± 1.2 kyr, which does not affect any of the conclusions drawn. The oldest boulder age is Kiwi 406 (19.1 ± 1.0 kyr).

Southeastern Australia

Barrows *et al.* (S*10, S11*) present a detailed study of LGM moraines in the Snowy Mountains and the Tasmanian highlands of southeastern Australia based on ^{36}Cl and ^{10}Be dating. They report a distinct “outermost LGM moraine” followed in some cases by a sequence of recessional moraines of

similar age. These authors report stratigraphic evidence for a rapid deglaciation (S*11*). Samples for ^{10}Be dating are reported from Blue Lake (9 samples), from Lake Cootapatamba (5 samples), from Poets Hill (2 samples), the Lake Dove moraine (2 samples), and the Lake Belton moraine (1 sample) in Tasmania.

The nineteen ^{10}Be ages (Table S3) range from 15.0 kyr to 19.1 kyr, with a mean of 16.8 ± 1.3 kyr. The oldest age reported for these moraines is 19.1 ± 1.8 kyr.

Lago Buenos Aires, Patagonia, and Chilean Lake District

Kaplan et al. (S*12*) present a cosmogenic study of the moraine sets fringing Lago Buenos Aires, Patagonia. Two distinct sets of moraine (Fenix II (older) and Fenix I (younger)) enclosing Lago Buenos Aires are both attributed to the last stage of the LGM (S*12, S13*). The distance between the outer Fenix II and the inner Fenix I terminal moraine crests is about 1.5 km.

The ^{10}Be ages for two boulders on the Fenix I moraine (S*12*) are 16.0 ± 0.4 kyr and 18.8 ± 1.5 kyr (Table S3, samples LBA-01), with a mean of 17.4 ± 1.9 kyr. Including the three boulders dated on the Fenix II moraine (Table S3, samples LBA-98) changes the mean to 18.4 ± 1.6 kyr. The oldest boulder age on Fenix II is 20.4 ± 0.7 kyr. For the conclusions below it is not critical whether or not to include Fenix II. The ages are again in agreement with the other records within uncertainties. For consistency reasons, we use the ages from the innermost LGM moraine, i.e. Fenix I, only.

Because these are so few results, this study is complemented by the LGM chronology from the nearby Chilean Lake District (42°S, 73°W, summarized in (S*14*)) where extensive geomorphic mapping (S*15*) and a detailed radiocarbon chronology (S*16*) yield a deglaciation age of 14,700 ^{14}C yr based on the mean of 72 dates with a spread of 700 ^{14}C yr, corresponding to about 17,900 calendar years (Intcal04).

2. Northern mid-latitude mountain glaciers

Bloody Canyon, Eastern Sierra Nevada

The field area is shown in Fig. S2. The LGM is mapped as two moraines designated Tioga 2 (early LGM) and Tioga 3 (late LGM) ((S*17, S18*) and Fig. S2). The Tioga 3 lateral moraine ridge is almost 100 m high and formed by vertical accretion, thus the age of the crest of the moraine almost certainly represents a close maximum age for the timing of LGM ice retreat. Inside the moraine loop, there is an ancient lake basin, implying major retreat following abandonment of the moraine by the glacier. In the Sierra Nevada there were two latest Pleistocene glacial readvances (Tioga 4 moraines, 15-13 kyr) (S*18*), but these were of minor extent compared to the LGM advances.

We dated four boulders on the Tioga 3 moraine crest, two from the left-lateral and two from the terminal area (Table S2). Ages range from 16.2 to 19.7 kyr, yielding a mean value of 17.8 ± 1.5 kyr. BC-19 yields the oldest age with 19.7±1.2 kyr. These ^{10}Be ages are consistent with earlier ^{36}Cl data from the Bloody Canyon Tioga 3 moraines (mean 16.4 ± 1.4 kyr, oldest 17.5 kyr) and with ^{36}Cl ages from the Tioga 3 moraine at nearby Bishop Creek (mean 17.7 ± 0.7 kyr, oldest 18.9 kyr). The ^{36}Cl data were earlier presented in (S*18*), and the exposure ages are here recalculated using current production rates (Table S4).

Fremont Lake Basin, Wind River Range, Wyoming

Gosse *et al.* (S*19*) present an extensive study from the moraines of the late Pinedale glaciation in Wyoming. The moraine morphology shows similarities to New Zealand's Lake Pukaki, with an LGM moraine complex lying outboard of a suite of LGM deglacial moraines, called "recessional" by these authors. Following Gosse et al. *(S19)*, we use the ten ^{10}Be dates of these recessional moraines to assess the timing of the LGM termination. The mean value of the ten ^{10}Be boulder ages on the recessional moraines is 17.6 ± 0.8 kyr, the small standard deviation reflecting the outstanding internal consistency of this data set (Table S3). The oldest boulder age within this set (sample 92-029) is 18.7 ± 0.6 kyr. A recent

paper by Benson et al. (S*20*) stresses the consistency between this data set and ^{36}Cl dated late Pinedale moraines in southern and northern Colorado.

Wallowa Mountains, Oregon

The LGM at this location is represented by the late Pinedale moraine damming Lake Wallowa (S*21*). These authors distinguish moraines of an older and a younger advance within a few hundred meters of each other.

They consider the following nine boulders to be the most representative for the younger advance: TTY 1, 3, 6, 13; WTO 1, 3, 4, 5, 9. The ^{10}Be dates of those samples yield a mean age of 16.8 ± 0.8 kyr. The oldest date within the age distribution is WTO-1 with a value of 18.0 ± 0.8 kyr (Table S3).

Northern Yellowstone ice cap, Montana

The LGM is represented here by the late Pinedale Eightmile terminal moraines; ten boulders were sampled for ^{10}Be analysis (S*22*), all of which are included here (Table S3). That paper (S*22*) reports LGM termination ages, based on the weighted mean of the ten ^{10}Be ages. These are younger than most of the records from similar sites. The authors conclude that there was a variable response of western US glaciers during the termination of the LGM.

The mean value of the ^{10}Be ages from nine boulders from the Eightmile moraine (8B, D, F, G, I, J, K, L, M; excluding outlier 8A) is 16.3 ± 1.2 kyr. The oldest age of this distribution is from sample 8-G with 18.8 ± 1.6 kyr. These values are somewhat younger than but, within uncertainties, are still consistent with the other records presented here.

Northern Switzerland

An expanded Rhone piedmont glacier system dominated the northern foreland of the Swiss Alps during the LGM. The terminal moraine complex near Wangen an der Aare has been attributed to the LGM maximum ice position of the Rhone glacier (S*23-S25*). Four giant boulders located on a single ridge in this moraine complex were dated

with ^{10}Be, ^{26}Al, and ^{36}Cl. The mean ^{10}Be age of the four boulders is 19.3 ± 1.8 kyr. Sample ER-2 provided the oldest age (20.8 ± 0.9 kyr). However, the sample sites lie on the outermost LGM moraines. The innermost LGM moraines are considered to be represented by the Solothurn moraine complex, about 5 km upstream of the Wangen an der Aare sample site (S*24*). The Solothurn moraines have not yet been cosmogenically dated, but the Wangen an der Aare dates provide a maximum age for the formation of the Solothurn moraines. We do not include them in the inter-hemispheric comparison but present them as an older maximum age for the LGM termination of the Swiss Alps.

Fig. S1. The LGM moraines alongside Lake Pukaki, New Zealand.

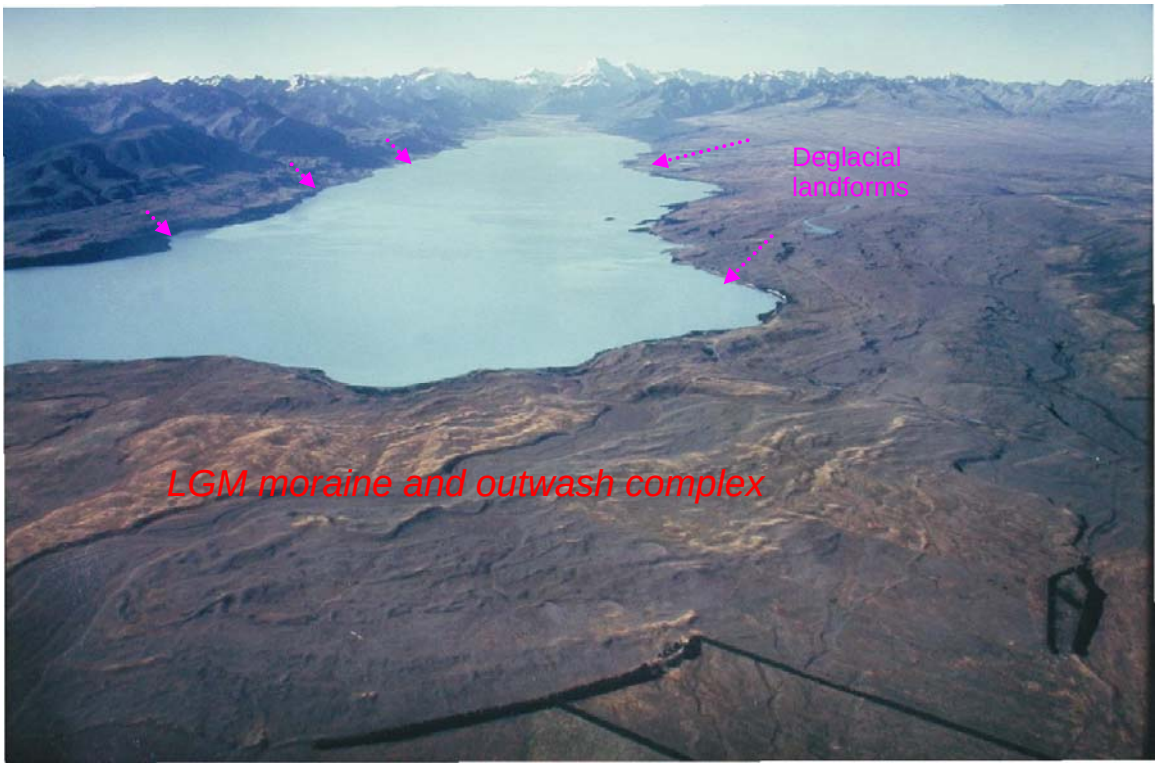

Fig. S2. Overview DEM of the Bloody Canyon area (courtesy of Prof. emeritus William A. Bowen). The termination of the Last Glacial Maximum is represented by the Tioga 3 moraine (yellow). The early LGM Tioga 2 moraine is shown in white. Deglaciation is indicated by the ancient lake basin inside the moraine. The upvalley moraine damming the lake is Tioga 4, dated at about 15 kyr ((S*18*), Schaefer unpublished) and thus yielding a minimum age for the Bloody Canyon termination.

Fig. S3. Example of a boulder (Kiwi 404) sampled on an inner LGM moraine alongside Lake Pukaki, New Zealand.

Table S1. ^{10}Be ages for the samples from the inner LGM and deglacial moraines, Lake Pukaki, Southern Alps, New Zealand. See also Fig. 1 and Figs. S1, S3.

Stated uncertainties are 1σ including analytical and blank errors. The mean of 18 procedural blanks (^{10}Be/^{9}Be = 2.5 * 10^{-14}) was used for blank correction; sample sizes were 40-90 g pure quartz separated from very fine-grained greywacke lithology. 0.25-0.4 mg of ^{9}Be-carrier were added (Spex-standard 1mg/ml Be).

The mean values (not weighted) of all the boulders are given in bold, together with the 1σ standard deviation. Samples Kiwi 524, 800 and 802 lie within the deglacial landform complex and are younger than the onset of deglaciation. Mean values for boulders on the moraine ridges outboard of the deglacial landforms represent a closely limiting maximum age for the LGM deglaciation. Their mean values are calculated with and without Kiwi 405 (the sample of lowest quality, see text). The oldest age within the maximum-limiting age population, Kiwi 406, is given in bold italic. "^{10}Be age" values in this table are corrected for sample thickness, landscape shielding and, where applicable, sample surface dip. See also 'supporting online materials'.

Sample Kiwi	Position*	Latitude/longitude/altitude	Height (m)	thickness (cm)	Shielding & Dip	^{10}Be (10^5 atoms/g)	^{10}Be age (kyr)
404	Term. LGM	44.179S/170.163E/580m	3	2.5	1	1.442 ± 0.087	18.8 ± 0.9
405	Term. LGM	44.181S/170.160E/580m	2	5.0	1	1.192 ± 0.079	15.0 ± 1.0
406	Term. LGM	44.180S/170.182E/590m	4	2.0	1	1.569 ± 0.079	***19.1 ± 0.8***
407	Term. LGM	44.181S/170.181E/600m	2	3.3	1	1.329 ± 0.040	16.2 ± 0.5
408	Term. LGM	44.181S/170.184E/570m	6	2.6	0.987	1.372 ± 0.086	18.4 ± 1.0
333	r.l. LGM	44.151S/170.114E/620m	6	3.5	1	1.514 ± 0.134	18.6 ± 2.0
336	r.l. LGM	44.155S/170.113E/610m	4	4.0	1	1.421 ± 0.150	17.6 ± 2.3
602	l.l. LGM	43.983S/170.247E/770m	4	5.0	1	1.533 ± 0.084	16.3 ± 0.8
603	l.l. LGM	43.983S/170.247E/770m	4	7.1	1	1.485 ± 0.102	16.2 ± 1.2
MEAN LGM	**Incl. 405**						**17.1 ± 1.2**
MEAN LGM	**Excl. 405**						**17.4 ± 1.0**
524	Deglacial	44.164S/170.218E/550m	3		0.997	1.120 ± 0.165	14.1 ± 1.8
800	Deglacial	43.998S/170.133E/540m	1.5	2.5	0.997	1.278 ± 0.03	16.4 ± 0.4
802	Deglacial	44.009S/170.127E/640m	1.5	2.3	0.997	1.327 ± 0.03	15.7 ± 0.4
Mean Deglacial							**15.4 ± 1.2**

*: 'Term. LGM': terminal LGM moraine; 'r.l. LGM': right lateral LGM moraine; 'l.l. LGM': left lateral LGM moraine;

Table S2. ^{10}Be ages for the late LGM (Tioga 3) moraine crest, Bloody Canyon, Eastern Sierra Nevada, USA. The lithology of the Bloody Canyon samples is biotite-rich granitic gneiss. For blank values, production rate parameters, correction factors and meaning procedures, see Table S1.

Sample	Position	Latitude/longitude/altitude	Height (m)	Sample thickness (cm)	Shielding & dip (%)	^{10}Be (10^5 atoms/g)	^{10}Be age (kyr)
BC-16	LGM Left lateral	37.887N/119.152W 2474m	1.5	5.0	0.956	4.708 ± 0.279	17.1 ± 1.0
BC-17	LGM Left lateral	37.887N/119.152W 2472m	1.5	2.3	0.956	4.542 ± 0.305	16.2 ± 1.1
BC-18	LGM Terminal	37.889N/119.145W 2401m	2	4.5	0.956	4.763 ± 0.336	18.2 ± 1.3
BC-19	LGM Terminal	37.889N/119.145W 2382m	1.5	3.0	0.956	5.192 ± 0.321	***19.7 ± 1.2***
MEAN							**17.8 ± 1.5**

Table S3. ^{10}Be data from earlier studies included in this survey together with geographic coordinates, sample thickness and production rate correction factors.

Sample	Altitude (m)	coordinates	thickness (cm)	Shielding/ Dip factor	^{10}Be (10^5 at g^{-1})
SOUTHERN HEMISPHERE					
SE Australia (S*10, S11*)					
BLS-001	1860	36.40S/148.32E	2.5	>0.99	3.24 ± 0.18
BLI-001	1850	36.40S/148.32E	5	>0.99	3.27 ± 0.17
BLI-002	1850	36.40S/148.32E	5	>0.99	2.76 ± 0.16
BLI-003	1850	36.40S/148.32E	4	>0.99	2.67 ± 0.15
BLH-008	1860	36.40S/148.32E	5	>0.99	3.51 ± 0.21
BLH-009	1860	36.40S/148.32E	5	>0.99	3.11 ± 0.18
BLH-013	1840	36.40S/148.32E	4	>0.99	3.24 ± 0.16
HLM-015	2010	36.40S/148.32E	1.8	>0.99	3.68 ± 0.17
LCI-001	2050	36.47S/148.27E	1.5	>0.99	3.45 ± 0.20
LCI-002	2050	36.47S/148.27E	2	>0.99	3.12 ± 0.41
LCI-004	2050	36.47S/148.27E	3	>0.99	3.46 ± 0.20
LCO-006	2020	36.47S/148.27E	1.8	>0.99	3.67 ± 0.22
LCO-007	2020	36.47S/148.27E	2	>0.99	3.34 ± 0.22
BLD-013	1840	36.40S/148.32E	4	>0.99	3.24 ± 0.16
MTF-043	1000	42.69S/146.54E	3.9	>0.99	1.72 ± 0.1
CDM-074	870	41.64S/145.95E	3.5	>0.99	1.79 ± 0.15
CDM-075	870	41.64S/145.95E	3.5	>0.99	1.62 ± 0.09
LKM-069	590	41.99S/145.56E	1.5	>0.99	1.43 ± 0.08
LKM-071	600	41.99S/145.56E	3.5	>0.99	1.24 ± 0.08
Patagonia (S*12*)					
LBA-01-05	438	46.60S/71.04W	1.5	1	1.194 ± 0.038
LBA-01-06	438	46.59S/71.94W	1.5	1	1.395 ± 0.110
LBA-98-78	454	46.63S/71.04W	1.5	1	1.374 ± 0.049
LBA-98-97	430	46.56S/71.03W	1.5	1	1.381 ± 0.051
LBA-98-98	430	46.56S/71.03W	1.5	1	1.502 ± 0.048
NORTHERN HEMISPHERE					
Wind River Range, Wyoming (S*19*)					
92-123	2369	42.93N/109.75W	3	1	5.34 ± 0.16
92-155	2375	42.93N/109.75W	2.5	1	5.35 ± 0.16
92-129	2390	42.93N/109.75W	5	1	5.61 ± 0.17
92-124	2337	42.93N/109.75W	5	1	5.03 ± 0.15
91-020	2352	42.93N/109.75W	5	1	5.03 ± 0.15
92-127	2335	42.93N/109.75W	4	1	5.04 ± 0.15
92-130	2341	42.93N/109.75W	5	1	5.41 ± 0.16
91-024	2323	42.93N/109.75W	10	1	5.02 ± 0.15
92-156	2341	42.93N/109.75W	5	1	5.28 ± 0.16
91-026	2342	42.93N/109.75W	4	1	4.68 ± 0.14

Sample	Altitude (m)	Coordinates	Sample thickness (cm)	Shielding & dip	^{10}Be (10^5 at g^{-1})
Wallowa Mnts, Oregon (S*21*)					
TTY-1B	1558	45.31N/117.19W	1.75	1	2.96 ± 0.18
TTY-3B	1542	45.32N/117.20W	1.75	1	2.98 ± 0.24
TTY-6A	1524	45.33N/117.20W	2	1	2.85 ± 0.21
TTY-13B	1439	45.34N/117.21W	1.75	1	2.74 ± 0.12
WTO-1B&C	1475	45.32N/117.22W	1.75	1	3.04 ± 0.14
WTO-3B	1466	45.33N/117.22W	1.75	1	2.65 ± 0.15
WTO-4A	1460	45.33N/117.22W	1.75	1	2.97 ± 0.13
WTO-5A	1454	45.33N/117.22W	1.75	1	2.82 ± 0.10
WTO-9B	1405	45.34N/117.22W	2	1	2.60 ± 0.16
North. Yellowstone, Montana (S*22*)					
8-B2	1550	45.43N/110.71W	2.5	1	2.59 ± 0.17
8-D1	1545	45.43N/110.71W	0.75	1	2.83 ± 0.16
8-F2	1544	45.44N/110.70W	1.5	1	3.08 ± 0.28
8-G2	1529	45.44N/110.70W	1	1	3.34 ± 0.28
8-I1&I2	1529	45.44N/110.69W	1.75	1	2.86 ± 0.12
8-J1&J2	1554	45.37N/110.69W	2	1	2.98 ± 0.25
8-K1	1536	45.43N/110.70W	2.75	1	2.91 ± 0.10
8-L1&L2	1554	45.37N/110.69W	3	1	2.71 ± 0.12
8-M2	1561	45.36N/110.69W	2.5	0	2.80 ± 0.11
Switzerland (max. LGM) (S*23*)					
ER 1	580	47.13N/7.63E	6	1	1.65 ± 0.10
ER 2	585	47.13N/7.63E	5	0.9	1.55 ± 0.07
ER 7	610	47.13N/7.63E	4	1	1.43 ± 0.10
ER 8	595	47.13N/7.63E	3	1	1.62 ± 0.10
TROPICS					
Bolivia/Peru (S*26*)*					
AL006	4390	11.07S/75.93W		0.97	8.17 ± 0.21
AL007	4391	11.07S/75.93W		0.99	6.59 ± 0.17
AL010	4384	11.07S/75.93W		0.98	7.82 ± 0.20
PE01-ALC-03	4390	11.07S/75.93W		0.95	6.95 ± 0.24
PE01-ALC-04	4390	11.07S/75.93W		0.95	7.22 ± 0.24
PE01-ALC-05	4383	11.07S/75.93W		0.95	9.45 ± 0.27
PE01-ALC-06	4383	11.07S/75.93W		0.95	7.02 ± 0.25
PE01-ALC-23	4376	11.07S/75.94W		0.95	6.74 ± 0.28
PE-01-ALC-24	4374	11.07S/75.94W		0.95	6.68 ± 0.38
PE-01-ALC-25	4364	11.07S/75.94W		0.95	6.63 ± 0.28
PE02-ALC-01	4377	11.07S/75.94W		0.97	6.90 ± 0.39
PE02-ALC-05	4380	11.07S/75.94W		0.97	6.58 ± 0.23

Sample	Altitude (m)	Coordinates	Sample thickness (cm)	Shielding & dip (%)	^{10}Be (10^5 at g^{-1})
PE01-ANT-01	4292	11.03S/75.95W		0.95	6.64 ± 0.23
-02	4296	11.03S/75.95W		0.93	6.97 ± 0.20
-03	4281	11.03S/75.95W		0.95	7.02 ± 0.21
-04	4281	11.03S/75.96W		0.94	7.23 ± 0.30
-05	4279	11.03S/75.95W		0.95	6.20 ± 0.21
-06	4279	11.03S/75.95W		0.95	6.32 ± 0.20
-07	4286	11.03S/75.95W		0.95	6.76 ± 0.25
PE01-CAL-01	4259	10.95S/75.99		0.94	6.24 ± 0.30
-02	4255	10.95S/75.99		0.95	6.04 ± 0.25
-03	4252	10.95S/75.99		0.95	7.48 ± 0.39
-04	4256	10.96S/75.99		0.94	5.98 ± 0.23
-05	4263	10.95S/75.99		0.95	5.65 ± 0.24
-06	4269	10.95S/75.99		0.91	6.11 ± 0.70
-07	4260	10.95S/75.99		0.95	5.93 ± 0.55
-08	4255	10.96S/76.00W		0.95	6.55 ± 0.21
-09	4259	10.96S/76.00W		0.95	6.83 ± 0.27
-10	4265	10.96S/76.00W		0.95	7.65 ± 0.26
-11	4252	10.96S/76.00W		0.95	7.27 ± 0.25
-12	4256	10.96S/76.00W		0.95	8.42 ± 0.75
-13	4267	10.97S/76.00W		0.95	7.10 ± 0.25
-14	4254	10.97S/76.00W		0.95	7.53 ± 0.27
ML-00-15	4643	16.32S/68.14W		0.95	8.44 ± 0.28
ZONG-03-01	3489	16.14S/68.18W		0.94	5.47 ± 0.28
-02	3500	16.14S/68.18W		0.92	4.81 ± 0.14
-03	3503	16.14S/68.18W		0.93	3.78 ± 0.13
-05	3505	16.14S/68.18W		0.95	4.10 ± 0.16
-06	3417	16.13S/68.17W		0.86	4.13 ± 0.16
-07	3408	16.13S/68.17W		0.85	4.02 ± 0.17
-09	3393	16.13S/68.17W		0.86	3.85 ± 0.10

*: These authors report a combined correction for sample thickness, topographic shielding and dip of the sampled surface.

Table S4. Updated ^{36}Cl chronology for the Tioga 3 moraines from Bloody Canyon and nearby Bishop Creek (S*18*), applying the production rate parameters given in refs (S*2, S27*).

Sample	^{36}Cl age (kyr)
Tioga 3, Bloody Canyon	
BC90-5	14.5
BC86-1	17.4
BC86-3	16.1
BC86-5	17.5
Tioga 3, Bishop Creek	
BPCR91-4	17.3
BPCR90-73	16.8
BPCR90-74	17.3
BPCR90-75	18.9
BPCR91-1	17.2
BPCR91-3	18.1
BPCR90-22	18.3
BPCR90-24	16.8
BPCR90-25	18.2
BPCR90-26	18.1
MEAN	**17.3 ± 1.1**

Supplementary References

S1. T. E. Cerling, H. Craig, *Annual Reviews of Earth Planetary Science Letters* **22**, 273 (1994).
S2. J. C. Gosse, F. M. Phillips, *Quaternary Science Reviews* **20**, 1475 (2001).
S3. M. D. Kurz, E. J. Brook, in *Dating in exposed and surface contexts* C. Beck, Ed. (University of New Mexico Press, 1994) pp. 139-159.
S4. D. Lal, *Earth and Planetary Science Letters* **104**, 424 (1991).
S5. J. Stone, *Journal of Geophysical Research* **105**, 23753 (2000).
S6. J. Dunne, D. Elmore, P. Muzikar, *Geomorphology* **27**, 3 (1999).
S7. J. Masarik, R. Wieler, *Earth and Planetary Science Letters* **216**, 201 (2003).
S8. H. S. Gair, *Mt. Cook sheet, Geological Map of New Zealand 1:250,000*, Wellington (1967).
S9. N. T. Moar, *New Zealand Journal of Ecology* **3**, 4 (1980).
S10. T. T. Barrows, J. O. Stone, L. K. Fifield, R. G. Cresswell, *Quaternary Science Reviews* **21**, 159 (2002).
S11. T. T. Barrows, J. O. Stone, L. K. Fifield, R. G. Cresswell, *Quaternary Research* **55**, 179 (2001).
S12. M. R. Kaplan, R. P. Ackert, B. S. Singer, D. C. Douglass, M. D. Kurz, *GSA Bulletin* **116**, 308 (2004).
S13. C. G. Caldenius, *Geografiska Annaler* **14**, 1 (1932).
S14. G. H. Denton, *Glacial and vegetational history of the Southern Lake District of Chile*, Geografiska Annaler A (1999), pp. 253.
S15. B. G. Andersen, G. H. Denton, T. V. Lowell, *Geografiska Annaler* **81 A**, 155 (1999).
S16. G. H. Denton *et al.*, *Geografiska Annaler* **81 A**, 107 (1999).
S17. M. I. Bursik, A. R. Gillespie, *Quaternary Research* **39**, 24 (1993).
S18. F. M. Phillips *et al.*, *Science* **274**, 749 (1996).
S19. J. C. Gosse, J. Klein, E. B. Evenson, B. Lawn, R. Middleton, *Science* **268**, 1329 (1995).
S20. L. Benson, R. Madole, G. Landis, J. Gosse, *Quaternary Science Reviews* **24**, 49 (2005).
S21. J. M. Licciardi, P. U. Clark, E. J. Brook, D. Elmore, P. Sharma, *Geology* **32**, 81 (2004).
S22. J. M. Licciardi *et al.*, *Geology* **29**, 1095 (2001).
S23. S. Ivy-Ochs, J. M. Schäfer, P. W. Kubik, H.-A. Synal, C. Schlüchter, *Eclogae Geologicae Helvetiae* **97**, 47 (2004).
S24. F. Nussbaum, *Mitteilungen der naturforschenden Gesellschaft Bern* **1761**, 141 (1910).
S25. A. Penck, E. Brueckner, *Die Alpen im Eiszeitalter*. Tauchnitz, Ed. (1901/09).
S26. J. A. Smith, G. O. Seltzer, D. L. Farber, D. T. Rodbell, R. C. Finkel, *Science* **308**, 678 (2005).
S27. F. M. Phillips, W. D. Stone, J. T. Fabryka-Martin, *Chemical Geology* **175**, 689 (2001).